Superconducting versus semiconducting electronic ground state in chirality-specific double-wall carbon nanotubes

2013 New J. Phys. 15 083021

(http://iopscience.iop.org/1367-2630/15/8/083021)

New Journal of Physics
The open access journal for physics

Superconducting versus semiconducting electronic ground state in chirality-specific double-wall carbon nanotubes

Ting Zhang[1,2] **and Ping Sheng**[1,2,3]

[1] Department of Physics, The Hong Kong University of Science and Technology, Clear Water Bay, Kowloon, Hong Kong, People's Republic of China

[2] Institute for Advanced Study, The Hong Kong University of Science and Technology, Clear Water Bay, Kowloon, Hong Kong, People's Republic of China

E-mail: sheng@ust.hk

New Journal of Physics **15** (2013) 083021 (18pp)
Received 29 April 2013
Published 8 August 2013
Online at http://www.njp.org/
doi:10.1088/1367-2630/15/8/083021

Abstract. By using two-loop renormalization group analysis, we explore the phase diagram with respect to the electron–phonon and Coulomb interaction strengths in the two (3,3)@(8,8) and (5,0)@(15,0) double-wall carbon nanotube systems (DWCNTs). Using estimation of the two types of coupling strengths from *ab initio* calculations, both systems are shown to scale to the superconducting fixed point as temperature decreases to zero. This is in contrast to the (3,3) and (5,0) single-wall carbon nanotubes, which scales to the Peierls-distorted semiconducting ground state. While the superconducting transition temperature can be quite low in the (3,3)@(8,8) system, the (5,0)@(15,0) promises observable superconducting behavior. Our result is in support of recent experimental observation of superconductivity in DWCNTs.

[3] Author to whom any correspondence should be addressed.

Contents

1. Introduction

The electronic ground state of metallic carbon nanotubes is an intriguing issue, owing to the non-unique implications offered by the electron–phonon interaction. It is well known that a one-dimensional (1D) metal can undergo a Peierls distortion, thereby leading to a semiconducting ground state. Recent *ab initio* calculations on single-wall carbon nanotubes have verified such predictions [1–6]. However, another possibility is the superconducting ground state. While there is no observation of superconductivity in a single, isolated single-wall carbon nanotube, there has been electrical, thermal specific heat and magnetic evidence of superconductivity in arrays of 4 Å carbon nanotubes embedded in the linear pores of aluminophosphate-five (AIPO4-5) zeolite crystals [7, 8]. Superconductivity has also been predicted and observed in ropes of carbon nanotubes, as well as in multi-wall carbon nanotubes [9–19]. Even in single-wall carbon nanotubes, several authors have also predicted a superconducting phase under special conditions [20–22]. More recently, it has been shown that if one takes into account the dielectric screening effect of the nanotube array (on the electron–electron interaction), a superconducting ground state can indeed be realized in (5,0) carbon nanotubes [23–25]. Furthermore, theoretical Monte Carlo simulations on the Ginzburg–Landau model have shown that with the appearance of the superconducting condensate, even a very weak Josephson coupling between the aligned nanotubes can lead to a 1D to 3D (three-dimensional) crossover transition at a temperature below that where the superconducting condensate first appears [8, 26].

In this work, we explore the ground state of metallic double-wall carbon nanotubes (DWCNTs), with the aim of examining the possibility of superconductivity in a *single* DWCNT. There is an important difference between a single 1D carbon nanotube and an array, because the latter can be viewed as altering the environmental dielectric constant of the system in which the

nanotube is situated; whereas for a single DWCNT we only have the interaction between the outer layer with one inner nanotube, and the fact that there is only a single layer makes the dielectric screening effectiveness not so apparent from the outset. Also, an array is known to offer the possibility of a 1D to 3D crossover which can suppress the Peierls distortion very effectively, which is absent for a single DWCNT.

Another motivation for this work arises from the experimental specific heat measurements on bulk DWCNT samples [27], which show that if one compares the Sommerfeld constant for the superconducting component of the sample to that of the metallic component of the sample, the ratio is found to be around 70%, i.e., most of the metallic DWCNTs can exhibit superconductivity at low temperatures. Such a high percentage implies a very general mechanism for suppressing the Peierls instability in metallic DWCNTs. Below we show that indeed, if both the inner and outer tubes are metallic, the screening of the Coulomb interaction between the electrons is sufficient to induce a superconducting ground state. Moreover, our results indicate a chirality-dependence in the superconducting transition temperature. This aspect also supports the experimental electrical and specific heat observations of a broad distribution of superconducting transition temperatures in bulk DWCNTs, ranging from 4 to 18 K [27].

Since it is accepted that the interaction between the inner and outer shells of a DWCNT is essentially van der Waals in character, the electronic structure of each shell may be treated as that of an isolated single-wall carbon nanotube. This is verified by Cohen and co-worker [19], in which (5,5)@(10,10) DWCNT has the band structure similar to the sum of individual (5,5) and (10,10) CNTs. However, the proximity of the two shells, separated by only 3.4 Å—the atomic separation between graphitic sheets—can mean a significant dielectric screening effect on the electron–electron interaction. This is especially the case if both shells are metallic in character. As renormalization group (RG) analysis is especially well-suited to examining the consequences of dielectric screening, we use this approach to study the two cases of (3,3)@(8,8) and (5,0)@(15,0) DWCNTs. We chose these two types of DWCNTs because both the inner and outer tubes in (3,3)@(8,8) and (5,0)@(15,0) are metallic. While for (3,3)@(8,8) DWCNT both shells are armchair and hence must be metallic; in the case of (5,0)@(15,0) the outer tube satisfies the usual rule of being metallic, while the inner tube is metallic owing to the very small radius and consequent σ–π mixing. So (5,0)@(15,0) is a typical representative of metallic zigzag DWCNTs, and (3,3)@(8,8) is representative for the armchair DWCNTs. Here the metallic nature of both inner and outer tubes is important because possible physical processes need a Fermi level in the system, and metallic tubes might provide reasonable screening for the electron–electron interactions. There is a second reason for choosing the above two DWCNTs for study, and that is because in both cases the inner tubes have a small radius and hence can offer strong electron–phonon interaction [28, 29], which plays a crucial role in the two physical processes—Peierls distortion and superconductivity—that are in competition. Our results show that in both (3,3)@(8,8) and (5,0)@(15,0) DWNT cases the superconducting order is the ground state, even though the transition temperatures may differ significantly. This, however, is in sharp contrast to the semiconducting ground state of the individual (3,3) and (5,0) CNTs due to the Peierls distortion, which is also analyzed by using the same approach. Our conclusion is consistent with the recent *ab initio* calculation that showed a superconducting ground state for the (5,5)@(10,10) DWCNT [19], as well as in support of the experimental observations [27].

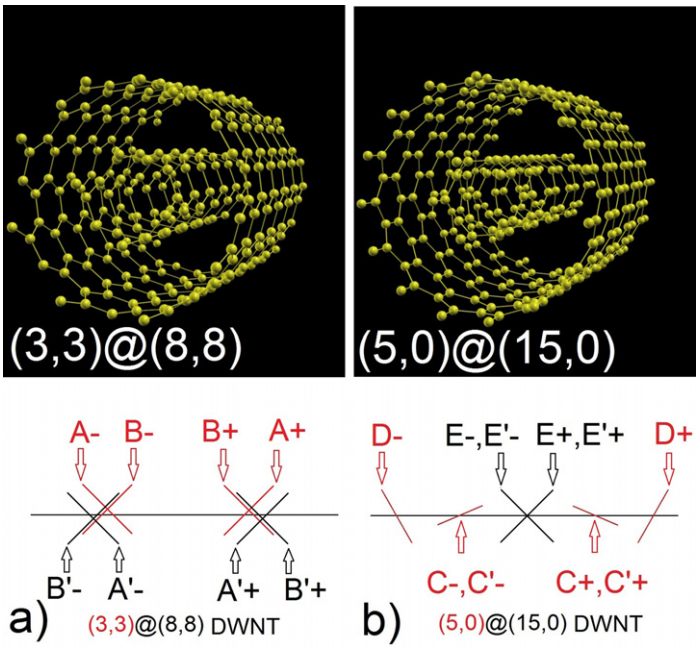

Figure 1. The atomic structure (upper panels) and linearized band structure near the Fermi level (lower panels) of (a) (3,3)@(8,8) DWCNT, and (b) (5,0)@(15,0) DWCNT. Bands of the inner tubes are plotted in red and those of the outer tube in black. In (a), the A,B bands belong to (3,3) while the A′,B′ bands belong to (8,8). The Dirac points of the inner and outer tubes are slightly different in energy. In (b), the degenerate C,C′ bands and D band belong to (5,0), while degenerate E,E′ bands belong to (15,0). Tunneling between inner and outer tubes is assumed to be negligible, and the band structure of the DWCNT is also assumed to not be modified by the inter-tube interactions. The Fermi energy is set to be a bit different from the Dirac point, so that we can neglect the Umklapp interactions.

2. Theoretical method

2.1. Residual electron–electron interactions in double-wall carbon nanotube (DWCNT)

To perform RG analysis, one needs to linearize the band structure near the Fermi energy. The linearized band structures are schematically illustrated in figure 1. We will neglect inter-tube tunneling, as well as assume that the Fermi energy is slightly off the crossing point of different bands, so as to avoid Umklapp interactions. The latter can occur either by doping, charge transfer between inner and outer tubes, or applied gate voltage. In $(n,n)@(n+5,n+5)$ DWCNTs, we shall assume the Dirac points of the inner and outer tubes to be slightly different in energy, which can be the result of a small charge transfer between the two shells [19].

There can be two types of residual interactions between electrons—the attractive phonon-mediated electron–electron interaction (PMI), and the repulsive Coulomb interaction. The total interaction is the sum of the two. To be specific, in figure 1 we label the bands of (3,3) CNT as A+, B+ around k_F, and A−, B− around $-k_F$. For the (8,8) CNT, the band structure is similar and hence its bands are labeled as A′± and B′±, respectively. For the zigzag (5,0) CNT, the

three bands are labeled as C,C′ and D, where C and C′ are the two degenerate bands with smaller Fermi momentum k_{FC}, and band D corresponds to the larger one k_{FD}. For the (15,0) CNT, we use E and E′ to label the degenerate bands associated with the two Dirac points. The electron–electron coupling vertex arises from two bands with opposite Fermi velocities, and in each there is a backward scattering coupling constant $g^{(1)}_{ijlk}$ and a forward scattering coupling constant $g^{(2)}_{ijkl}$. The two can transform into each other by exchanging the outgoing electrons. Here $i, j, k, l = \mathrm{A}, \mathrm{A}' \ldots \mathrm{E}'$ denotes the index of band associated with the two scattering electrons, and the scattering process is $k \to i$, $l \to j$ in the backward direction and $l \to i$, $k \to j$ in the forward process. Hence we can identify the couplings $g^{(1)}_{\mathrm{A+A-A+A-}}$ and $g^{(2)}_{\mathrm{A+A-A-A+}}$ in the (3,3)@(8,8) system as the backward and forward scatterings in band A of the inner (3,3) CNT, respectively. Similarly the couplings $g^{(1)}_{\mathrm{D+D-D+D-}}$ and $g^{(2)}_{\mathrm{D+D-D-D+}}$ in (5,0)@(15,0) denote the backward and forward scatterings in band D of the inner (5,0) CNT. The above two sets of coupling channels are the most important ones because they generate the most divergent response functions in the RG flow (see below). The sign of a coupling constant is defined to be negative if the coupling is attractive and positive if the coupling is repulsive. The value of each coupling constant is expressed in units of Fermi velocity. Detailed definitions of all the coupling constants can be found in appendix A.

2.2. *Estimation of the initial (un-renormalized) values of electron–electron interactions*

We use the *ab initio* estimation [1, 24, 25] of the PMIs and the bare values of the Coulomb interactions for the (3,3) and (5,0) CNTs. For the outer (8,8) CNT, we note that the strength of both the phonon-mediated and direct electron–electron interactions follow the $1/R$ scaling [28, 29], where R is the CNT radius. Hence we can estimate the initial values of (8,8) CNT from the corresponding ones of (3,3). For the (15,0), since the band structure is different from the (5,0), we employ the method of Egger [29] and Kaxiras and co-workers [30] to estimate the bare couplings. The key point in our analysis is to estimate the screening effect between the inner and outer tubes.

The bare values of the inter-tube Coulomb interaction are similar to that for the intra-tube interaction [29]

$$V_{\text{inter-tube}}(r - r') = \frac{e^2/\kappa}{\sqrt{(x - x')^2 + 4R^2 \sin^2\left[(y - y')/2R\right] + a_z^2}}, \tag{1}$$

where e is the electronic charge, $\kappa \sim 2$ is the environmental dielectric constant (taking into account all the bonded electrons inside graphite sheet), x the coordinate along the tube axis and y the coordinate along tube's circumference. For intra-tube potential, R is the tube radius and $a_z \sim 1.6$ Å is the size of the π orbital. To estimate the inter-tube potential, we take R to be the average radius of the inner and outer tubes, and $a_z \sim 5$ Å (obtained from $1.6 + 3.4$ Å) to be the minimum distance between two electrons, each associated with either the inner tube or the outer tube. Since the Coulomb potential is only a function of $r - r'$, we can integrate y and y' and perform a Fourier transform on $V(x - x')$ to obtain $V(q)$. The bare Coulomb potential $V(q)$ is very large around $q \sim 0$, where its magnitude is about $16/\kappa$ for (3,3) CNT and $50/\kappa$ for the (5,0) CNT. This is unfavorable for the appearance of superconductivity. However, owing to the screening effect, the inner and outer tubes will mutually and strongly renormalize the Coulomb

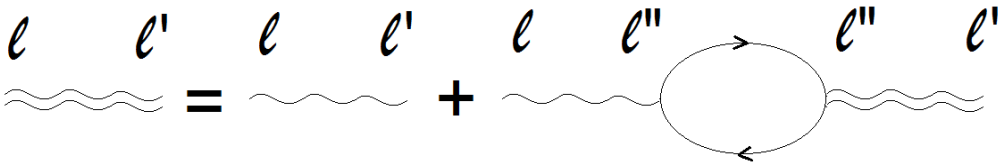

Figure 2. Feynman diagram of the screening in forward Coulomb interactions. A single wiggly line denotes the bare Coulomb interaction and double wiggly lines denote the screened interaction. Solid lines are the Green functions of electrons. l, l' and l'' here denote either the inner or the outer tube. It should be noted that l'' should not be equal to l, since the electron–electron interaction should be screened by the other tube, but not by itself.

interaction between the electrons. This effect can be evaluated by using the Dyson equations [24, 25, 31], graphically shown in figure 2:

$$\begin{aligned} V_{\mathrm{ii}}^{(r)}(q) &= V_{\mathrm{ii}}(q) + \Pi_{\mathrm{o}} V_{\mathrm{io}}(q) V_{\mathrm{oi}}^{(r)}(q), \\ V_{\mathrm{oo}}^{(r)}(q) &= V_{\mathrm{oo}}(q) + \Pi_{\mathrm{i}} V_{\mathrm{oi}}(q) V_{\mathrm{io}}^{(r)}(q), \\ V_{\mathrm{io}}^{(r)}(q) &= V_{\mathrm{io}}(q) + \Pi_{\mathrm{o}} V_{\mathrm{io}}(q) V_{\mathrm{oo}}^{(r)}(q), \\ V_{\mathrm{oi}}^{(r)}(q) &= V_{\mathrm{oi}}(q) + \Pi_{\mathrm{i}} V_{\mathrm{oi}}(q) V_{\mathrm{ii}}^{(r)}(q), \end{aligned} \tag{2}$$

where the subscripts i,o denote the inner or outer tube, respectively, and the superscript r denotes screened potential. V_{ii} and V_{oo} are the intra-tube Coulomb potentials in inner and outer tubes, while $V_{\mathrm{io}} = V_{\mathrm{oi}}$ being the inter-tube potential. The symbols Π_{i} and Π_{o} stand for the polarizability of the inner and outer tubes, respectively. For 1D electron gas the polarizability is given by $\Pi(q) = -2/\pi\upsilon_{\mathrm{F}}$ (see appendix B). It should be noted that $V_{\mathrm{io}}^{(r)}$ and $V_{\mathrm{oi}}^{(r)}$ are not equal because the screening capabilities of the inner and outer tubes are different. Equation (2) is associated with the forward scattering processes, since Π_{i} and Π_{o} have finite values only in such processes. Generally speaking, the screening effect due to the double-shell structure can greatly reduce the Coulomb interaction at $q \sim 0$, and this reduction can lead to significant consequences in deciding the ground state of the DWCNT. The resulting screened Coulomb potential is about 0.68 for (3,3) CNT and 0.58 for (5,0) CNT at $\kappa = 2$. These values are about two orders of magnitude smaller than the bare values. Such significant screening effect, associated with one single layer of carbon atoms in a metallic carbon nanotube, has been noted in an earlier *ab initio* calculation [32]. Moreover, we find the Coulomb interaction reduction in the inner tube to be larger than that in the outer tube, in agreement with the intuitive picture since for the outer tube the electric field lines can freely extend outward into the environment, whereas for the inner tube the screening is rather complete. The bare and screened Coulomb potentials, and the phonon-mediated attractive coupling constants, are shown in table A.1 in appendix A.

2.3. Second order renormalization group treatment of the DWCNT system

Usually the metallic CNTs are considered as Luttinger liquid (LL) [33–39], and there are many works on this topic [29, 40–42]. However the LL model is valid for the region of electron–electron interaction that is repulsive, as backward scattering is irrelevant in this case.

The LL model represents the fixed point of the RG analysis if interactions between electrons are repulsive. With the consideration of phonon-mediated interaction, however, the net interaction between electrons can be attractive if the Coulomb interaction is well screened. Under this condition, the system will scale to the so-called 'strong coupling' fixed point, in which all coupling constants go to infinity if only the first order RG is applied [42–47]. To avoid infinities in coupling constants and the resulting unphysical 1D 'phase transition' at finite temperatures [42–49], we employ two-loop RG method [42–47] to analyze the ground state of the DWCNT systems. The method to derive the scaling equations for the coupling constants is described in appendix C. We consider four types of response functions [42–47]: the charge density wave (CDW) N, the spin density wave (SDW) χ, the singlet superconductivity (SS) $\Delta_{\rm S}$, and the triplet superconductivity (TS) $\Delta_{\rm T}$. We follow the standard RG treatment to obtain the following scaling equations for these response functions:

$$\begin{aligned}
\frac{{\rm d}\ln \overline{N_n}(\omega/E_0)}{{\rm d}\ln(\omega/E_0)} &= \frac{1}{\pi \upsilon_{\rm F}}(2g_n^1 - g_n^2),\\
\frac{{\rm d}\ln \overline{\chi_n}(\omega/E_0)}{{\rm d}\ln(\omega/E_0)} &= \frac{1}{\pi \upsilon_{\rm F}}(-g_n^2),\\
\frac{{\rm d}\ln \overline{\Delta_{{\rm S}n}}(\omega/E_0)}{{\rm d}\ln(\omega/E_0)} &= \frac{1}{\pi \upsilon_{\rm F}}(g_n^1 + g_n^2),\\
\frac{{\rm d}\ln \overline{\Delta_{{\rm T}n}}(\omega/E_0)}{{\rm d}\ln(\omega/E_0)} &= \frac{1}{\pi \upsilon_{\rm F}}(-g_n^1 + g_n^2).
\end{aligned} \tag{3}$$

Here n is the vertex index and the over-bar means the response functions in the equations are actually the auxiliary function of response functions [42–47]. E_0 is the cutoff energy used in RG treatment. $\omega < E_0$ is the energy scale or temperature and $\omega \to 0$ in the scaling process. For the (3,3) CNT, we consider the response functions associated with the vertices $g_{\rm A+A-A-A+}$ and $g_{\rm A+B+B+A+}$, corresponding to $q = 2k_{\rm FA}$ and 0, respectively. For the (5,0) CNT, we consider the response functions associated with the vertices $g_{\rm C+C-C-C+}$ and $g_{\rm D+D-D-D+}$, corresponding to $q = 0$ in the superconducting channel and $q = 2k_{\rm FC}$ or $2k_{\rm FD}$ in the CDW/SDW channels, respectively. As the coupling constants approach their fixed point values, the response functions are power-law divergent, $(\omega/E_0)^X$, as $\omega \to 0$ and the power exponent X is determined by the right-hand sides of equation (3). Since $X < 0$, it is noted that the larger the absolute value of X, the corresponding response function is more divergent in scaling to lower energies. The divergence in response functions signals a phase transition. The most divergent response function determines the ground state of the system, since by definition, the larger the response function implies the larger the order parameter as the result of a small perturbative disturbance. Hence the state with the most divergent response will be what is measured experimentally. An infinite response function means there is a second order phase transition. In our case the response functions diverge at zero temperature, which agrees with the Hohenberg–Mermin theorem [48, 49] that in 1D a phase transition can occur only at $T = 0$. In contrast, first order RG suffers from the unphysical divergence in response functions at finite temperatures.

3. Results and discussion

3.1. Ground state for the armchair $(n,n)@(n+5,n+5)$ DWCNTs

Our results show that for the (3,3)@(8,8), the Coulomb interaction is strongly suppressed at $q = 0$, by about one magnitude from their bare values. The fixed point is presented in table A.1 in appendix A. The response functions in both the inner (3,3) and the outer (8,8) are the same. The most divergent response function is in the SS channel, $\Delta_{S,A+A-A-A+}(q = 0) \sim (\omega/E_0)^{-3.28}$, while the next divergent one is in the CDW channel, $N_{A+A-A-A+}(q = 2k_{FA}) \sim (\omega/E_0)^{-2.72}$. The behaviors of other response functions are shown in appendix D. It follows that the (3,3)@(8,8) DWCNT should be superconducting at zero temperature because of the screening effect. However, we must note that the energy scale at which that coupling constants reach their fixed-point values is extremely low in this case. In the inner (3,3), the crossing occurs at around $\ln(\omega/E_0) \sim -12$, while in the outer (8,8) this value is even lower. So it may be difficult to see observable superconductivity in the $(n,n)@(n+5,n+5)$ DWCNT systems in experiment. This is consistent with the result of Cohen and co-worker [19], in which the superconducting transition temperature of (5,5)@(10,10) is estimated to be lower than 1 K. The reason for such an extremely low transition energy scale is that the PMI is weak. However, if the Coulomb interaction can be further screened by environmental dielectric constant κ, then the situation can be different as shown in figure 4(b). For different n index DWCNT—$(n,n)@(n+5,n+5)$—since the PMI and the Coulomb interaction are both inversely proportional to the radius R, we can expect their transition temperatures to be even lower. This is also shown in figure 4(b). The assumption, that $g_{A+B'+A'+B+}$and $g_{A+A'-B'-B+}$ are prohibited by momentum conservation, is important in our calculations since otherwise such backward scatterings will make the system scale to a CDW ground state. The charge-transfer-induced band structure hence plays an important role in generating a superconducting ground state in the $(n,n)@(n+5,n+5)$ DWCNTs [19].

For comparison with the DWCNTs, we have also calculated the same response functions for a single (3,3) CNT with no outer tube to screen the Coulomb potential. In this case the CDW in the $q = 2k_{FA}$ channel, $N_{A+A-A-A+}(q = 2k_{FA})$, with a power exponent -5.04, is the most divergent. Both the CDW and SS response functions in band A are shown in figure 3(a). We note that the coupling constants fall into their fixed point values at around $\ln(\omega/E_0) \sim -10$. Therefore in contrast to the (3,3)@(8,8) DWCNT, the ground state order for a single (3,3) CNT is the semiconducting Peierls CDW.

3.2. Ground state for the (5,0)@(15,0) DWCNT

Next we consider the (5,0)@(15,0) DWCNT system. In a free-standing (5,0) CNT, only the CDW/SDW response functions around the nesting vectors $q = 2k_{FC}$ and $2k_{FD}$, plus the superconducting response functions around $q = 0$ need to be considered. As a result, the CDW order around $q = 2k_{FD}$, $N_{D+D-D-D+}(q = 2k_{FD}) \sim (\omega/E_0)^{-10.43}$, is the most divergent, and the SS/TS response function do not diverge at all, hence a single (5,0) CNT is strongly favored to undergo a Peierls transition. This is consistent with the earlier results [1–6, 23].

However if the (5,0) CNT is embedded in a metallic (15,0) CNT, the screening effect again greatly modifies the result. Among response functions the SS response in band D $\Delta_{S,D+D-D-D+}(q = 0) \sim (\omega/E_0)^{-3.48}$, is the most divergent, while the next divergent one is in the CDW channel, $N_{D+D-D-D+}(q = 2k_{FD}) \sim (\omega/E_0)^{-2.52}$. This is shown in figure 3(d). Other

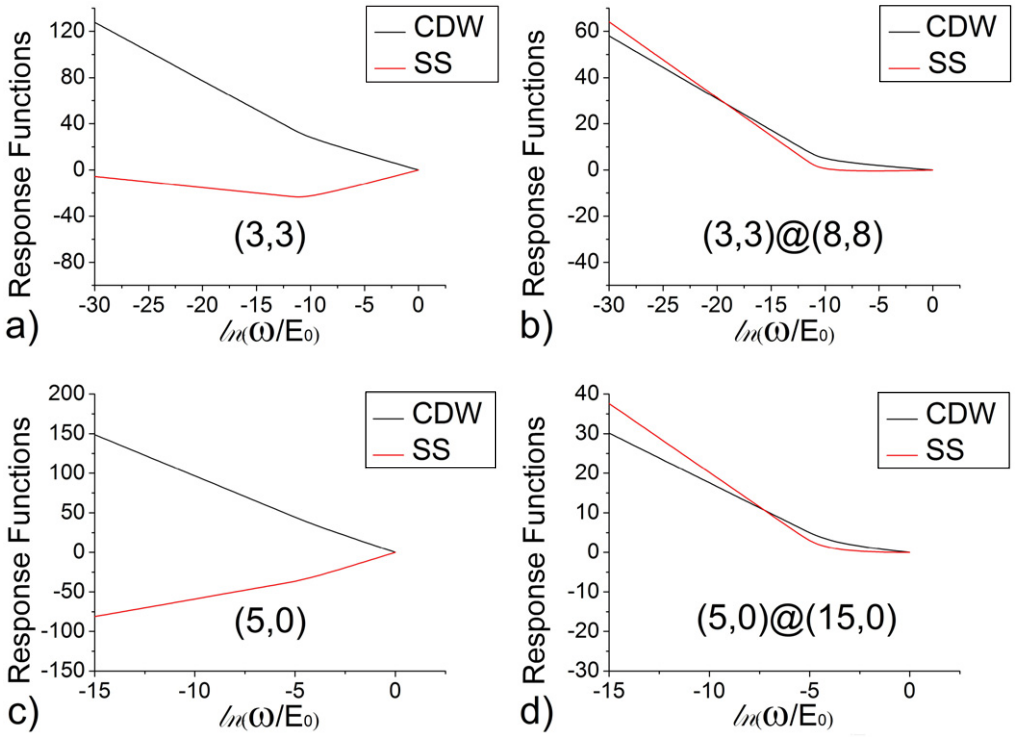

Figure 3. The most divergent CDW and SS response functions calculated under the condition of $\kappa = 2$. The x-axis is the energy scale or temperature, and the scaling direction is from right to left, toward decreasing energy scale. $T \to 0\,\mathrm{K}$ is at $\ell n(\omega/E_0) \to -\infty$. The y-axis is the log of response functions' amplitudes. The case of single-wall (3,3) CNT is shown in (a). It is seen that Peierls distortion/CDW order is always dominant. The case of (3,3)@(8,8) DWCNT (for the (3,3) part) is shown in (b). It is seen that the SS order dominates, but the crossing occurs at very low temperatures. The case of the single-wall (5,0) CNT is shown in (c), and it is seen that the Peierls distortion/CDW order is always dominant. The case of (5,0)@(15,0) (for the (5,0) part) is shown in (d). It is seen that the SS order is the ground state, and the crossing occurs at a relatively higher temperature than that in (b).

response functions' behaviors are shown in appendix D. It is noted that at higher temperatures (energies), the CDW order is the largest until $\ln(\omega/E_0) \sim -7$, then the SS order dominates. If we estimate the initial cutoff energy to be $\sim$0.1 eV, then $\ln(\omega/E_0) \sim -7$ implies the energy scale to be about 1/1000 of the initial energy cutoff. That means one may expect the appearance of superconducting condensate at $\sim$1 K. Although this temperature is still quite low, higher superconducting temperatures are possible if better screening is provided. For example, with an environment dielectric constant >2, or if the DWCNT is embedded in a bundle (such is just the case in [27]). A phase diagram of the relevant crossing energy scale, plotted as a function of $\boldsymbol{\kappa}$, is shown in figure 4(a).

By comparing the phase diagram of the $(n,n)@(n+5,n+5)$ and the (5,0)@(15,0) DWCNT, we find that although the $(n,n)@(n+5,n+5)$ DWCNTs are superconducting at $T = 0$, the actual crossing temperature at which superconducting order dominates is extremely

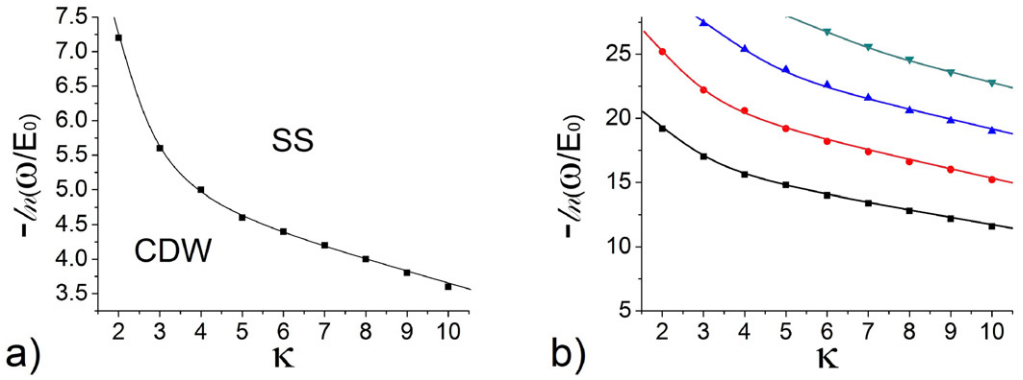

Figure 4. The CDW/SS crossing point plotted as a function of environment dielectric constant κ. (a) is for the case of (5,0)@(15,0) DWCNT and (b) the case of (n,n)@$(n+5,n+5)$ DWCNTs. The y-axis is the energy scale $-\ln(\omega/E_0)$, and the temperature $T\to 0$ as $y\to\infty$. The dots denote the crossing points at which the SS order exceeds the CDW order, below which (temperature) we can expect superconducting behavior. In (5,0)@(15,0) DWCNT, if κ is large, we can expect a higher superconducting transition temperature, while in (n, n)@$(n+5, n+5)$, such crossing points are at extremely low temperatures. The color dots and lines in (b) stand for different DWCNTs: black squares denote (3,3)@(8,8), red circles denote (4,4)@(9,9), blue triangles denote (5,5)@(10,10) and dark green triangles denote (6,6)@(11,11).

low so that even by embedding in a high-κ dielectric medium the actual observation could be difficult. However, in (5,0)@(15,0) the additional environmental screening can be very effective in enhancing the crossing temperature of SS over CDW. If one estimates the crossing temperature to be $\sim$1 K at $\kappa = 2$, then it can be enhanced to $\sim$30 K at $\kappa = 10$. The temperature at which the SS order exceeds the CDW order is much higher in the (5,0)@(15,0) DWCNT than in the (n,n)@$(n+5,n+5)$ DWCNT. This difference is due to the fact that in (5,0)@(15,0) DWCNT the phonon-mediated electron–electron interaction is stronger than that in (n, n)@$(n+5, n+5)$ DWCNTs. In the (3,3)@(8,8) DWCNT, the phonon-mediated interaction is about -0.3 in the coupling channel $g^{(1)}_{\mathrm{A+A-A+A-}}$, while for the (5,0)@(15,0) DWCNT, the corresponding phonon-mediated interaction is about -1.1 in the channel $g^{(1)}_{\mathrm{D+D-D+D-}}$. Combining with the residue Coulomb interaction, we can see at $\kappa = 2$, the (5,0)@(15,0) system has an attractive coupling for about twice the strength as the (3,3)@(8,8). So it is not surprising that (5,0)@(15,0) has a much higher cross-over energy (temperature).

4. Concluding remarks

In conclusion, we find that in (3,3)@(8,8) and (5,0)@(15,0) DWCNTs, the outer tube can stabilize the inner tube against the Peierls distortion, so that the ground state of the inner tube is superconducting. This is in contrast to single (3,3) and (5,0) CNTs, which are strongly favored to undergo a Peierls transition and hence will have a semiconducting ground state.

By considering two types of chiralities, we have found that (i) screening is the common mechanism for inducing the superconducting ground state, and (ii) the strength of

electron–phonon interaction is the distinguishing feature for determining the widely different transition temperatures. In future, if there are first-principle calculations that can provide the initial values for other types of chiral carbon nanotubes, the same method can be applied to determine the stability of the superconducting ground state as well. However, that is not expected to alter the two conclusions stated above. Furthermore, it is noted that our result provides a reasonable explanation for the high percentage of metallic DWCNTs observed to be superconducting at low temperatures [27]. The significant difference in the crossover energy for the armchair versus zigzag metallic DWCNTs also supports the observed broad distribution in the transition temperature [27].

Acknowledgments

We acknowledge the support of SRFI11/SC02 and HK RGC grant HKUST9/CRF/08 for this work.

Appendix A. Definition of coupling constants, initial values and fixed points

By taking into account momentum conservation, we identify 8 interaction vertices in the (3,3)@(8,8) DWCNT and 12 interaction vertices in the (5,0)@(15,0) DWCNT. In the (3,3)@(8,8), the 3 interaction vertices are the inner tube ones—$g_{\mathrm{A+A-A-A+}}$, $g_{\mathrm{A+B+B+A+}}$, $g_{\mathrm{A+A-B+B-}}$, 3 are from the outer tube—$g_{\mathrm{A'+A'-A'-A'+}}$, $g_{\mathrm{A'+B'+B'+A'+}}$, $g_{\mathrm{A'+A'-B'+B'-}}$ and 2 are from the inter-tube coupling vertices—$g_{\mathrm{A+A'-A'-A+}}$, $g_{\mathrm{A+B'+B'+A+}}$. Since we assume the tunneling between inner and outer tubes to be negligible, the corresponding two coupling constants vanish. Also, the backward scatterings $g_{\mathrm{A+B'+A'+B+}}$ and $g_{\mathrm{A+A'-B'-B+}}$ between the inner and outer tubes are prohibited by momentum conservation. The momentum transfer between A+, B+ is not the same as between A′+, B′+. This is because the Dirac points of inner and outer tubes are slightly different in energy. With two coupling constants per vertex, hence in (3,3)@(8,8) there are a total of 14 non-zero coupling constants. Similarly, in the (5,0)@(15,0) DWCNT there are a total of 21 non-zero coupling constants, with 12 from the inner tube vertices, 6 from the outer tube vertices, and 3 from inter-tube coupling.

Appendix B. Evaluation of the polarizability

The polarizability of a 1D electron gas is given by

$$\Pi(q) = \frac{2}{L}\sum_{k}\frac{f(\varepsilon_{k+q}) - f(\varepsilon_k)}{\varepsilon_{k+q} - \varepsilon_k}. \tag{B.1}$$

Here $L = Na$ is the length of CNT, a is the lattice constant, N being the number of cells inside the 1D metal, f denotes the Fermi distribution function and ε_k is the energy dispersion of the band. Hence, alternatively, we write

$$\Pi(q) = \frac{2}{2\pi}\left(\frac{2\pi}{Na}\right)\sum_{k}\frac{f(\varepsilon_{k+q}) - f(\varepsilon_k)}{\varepsilon_{k+q} - \varepsilon_k}. \tag{B.2}$$

Table A.1. The initial values adapted in the scaling equations and the corresponding fixed points. For individual (3,3) and (5,0) CNTs, we used the bare values plus the phonon mediated values; while for DWCNTs we used the screened values plus phonon-mediated values. Our initial values are based on the estimates from [24, 25]. For (3,3) and (5,0) CNTs, the initial values are directly adapted from [24, 25], obtained from tight-banding calculations. The electron–phonon interaction of (3,3) is estimated from *ab initio* calculations from [1] For (8,8) CNT and other (n,n) CNTs, the initial values can be calculated with the corresponding (3,3) ones using the relation $g \sim 1/R$. For (15,0), whose initial coupling constants are not given in [24, 25], we have used the method described in [28] and appendix E in [30] to calculate the initial values.

	Single CNT case initial values: (bare Coulomb potential+PMI)	Fixed points	Double-wall CNT case initial values: (screened potential+PMI)	Fixed points
V_{ii} in (3,3) CNT			$V_{ii}^{(r)}$ in (3,3) CNT, in (3,3)@(8,8) at $\kappa = 2$	
$g^2_{A+A-A-A+}/\upsilon_{FA}$	$15.97/\kappa - 0.05$	3.27	$0.68 - 0.05$	−4.01
$g^2_{A+B+B+A+}/\upsilon_{FA}$	$15.97/\kappa - 0.05$	9.56	$0.68 - 0.05$	2.27
Backscattering in (3,3) CNT			Backscattering in (3,3) CNT, in (3,3)@(8,8)	
$g^1_{A+A-A+A-}/\upsilon_{FA}$ $g^2_{A+A-B+B-}/\upsilon_{FA}$	$0.06/\kappa - 0.3$	−6.28	$0.06/\kappa - 0.3$	−6.28
$g^1_{A+B+A+B+}/\upsilon_{FA}$	$0.23/\kappa - 0.05$	0	$0.23/\kappa - 0.05$	0
$g^1_{A+A-B-B+}/\upsilon_{FA}$	$0.23/\kappa - 0.05$	−6.28	$0.23/\kappa - 0.05$	−6.28
V_{oo} in (8,8) CNT			$V_{oo}^{(r)}$ in (8,8) CNT, in (3,3)@(8,8) at $\kappa = 2$	
$g^2_{A'+A'-A'-A'+}/\upsilon_{FA}$ (V_{oo})	$13.73/\kappa - 0.019$	N/A	$0.70 - 0.019$	−4.01
$g^2_{A'+B'+B'+A'+}/\upsilon_{FA}$ (V_{oo})	$13.73/\kappa - 0.019$	N/A	$0.70 - 0.019$	2.27
Backscattering in (8,8) CNT			Backscattering in (8,8) CNT, in (3,3)@(8,8)	
$g^1_{A'+A'-A'+A'-}/\upsilon_{FA}$	$0.022/\kappa - 0.11$	N/A	$0.022/\kappa - 0.11$	−6.28
$g^2_{A'+A'-B'+B'-}/\upsilon_{FA}$				
$g^1_{A'+B'+A'+B'+}/\upsilon_{FA}$,	$0.086/\kappa - 0.019$	N/A	$0.086/\kappa - 0.019$	0
$g^1_{A'+A'-B'-B'+}/\upsilon_{FA}$	$0.086/\kappa - 0.019$	N/A	$0.086/\kappa - 0.019$	−6.28
V_{io}, V_{oi} in (3,3)@(8,8)			$V_{io}^{(r)}$, $V_{oi}^{(r)}$ in (3,3)@(8,8) at $\kappa = 2$	
$g^2_{A+A'-A'-A+}/\upsilon_{FA}$, $g^2_{A+B'+B'+A+}/\upsilon_{FA}$	$13.25/\kappa$	N/A	0.73, 0.87[a]	0.73
V_{ii} in (5,0) CNT			$V_{ii}^{(r)}$ in (5,0) CNT, in (5,0)@(15,0) at $\kappa = 2$	
$g^2_{C+C-C-C+}/\upsilon_{FC}$, $g^2_{C+D+D+C+}/\upsilon_{FC}$	$50.83/\kappa$	26.47	0.58	1.63

Table A.1. (Continued.)

$g^2_{D+D-D-D+}/\upsilon_{FC}$, $g^2_{C+C'-C'-C+}/\upsilon_{FC}$	$50.83/\kappa$	20.18	0.58	−4.65
Backscattering in (5,0) CNT			Backscattering in (5,0) CNT, in (5,0)@(15,0)	
$g^1_{C+C-C+C-}/\upsilon_{FC}$	$3.6/\kappa - 0.6$	0	$3.6/\kappa - 0.6$	0
$g^1_{C+C'-C'+C-}/\upsilon_{FC}$	$3.6/\kappa - 0.6$	−6.28	$3.6/\kappa - 0.6$	−6.28
$g^1_{D+D-D+D-}/\upsilon_{FC}$	$1.1/\kappa - 1.1$	−6.28	$1.1/\kappa - 1.1$	−6.28
$g^2_{C+C'-C-C'+}/\upsilon_{FC}$, $g^1_{C+C'-C+C'-}/\upsilon_{FC}$	$0.05/\kappa - 0.5$	−6.28	$0.05/\kappa - 0.5$	−6.28
$g^1_{C+D+C+D+}/\upsilon_{FC}$, $g^1_{C+C'-D-D+}/\upsilon_{FC}$	$0.5/\kappa - 0.5$	0	$0.5/\kappa - 0.5$	0
$g^2_{C+C'-D+D-}/\upsilon_{FC}$	$0.5/\kappa - 0.5$	−6.28	$0.5/\kappa - 0.5$	−6.28
	$0.3/\kappa - 0.5$	−6.28	$0.3/\kappa - 0.5$	−6.28
V_{oo} in (15,0) CNT			$V^{(r)}_{oo}$ in (15,0) CNT, in (5,0)@(15,0) at $\kappa = 2$	
$g^2_{E+E-E-E+}/\upsilon_{FC}$	$43.89/\kappa$	N/A	1.98	3.26
$g^2_{E+E'-E'-E+}/\upsilon_{FC}$	$43.89/\kappa$	N/A	1.98	−3.02
Backscattering in (15,0) CNT			Backscattering in (15,0) CNT, in (5,0)@(15,0)	
$g^1_{E+E-E+E-}/\upsilon_{FC}$	$1.16/\kappa$	N/A	$1.16/\kappa$	0
$g^1_{E+E'-E+E'-}/\upsilon_{FC}$	$1.16/\kappa$	N/A	$1.16/\kappa$	−6.28
$g^1_{E+E'-E'+E-}/\upsilon_{FC}$, $g^2_{E+E'-E-E'+}/\upsilon_{FC}$	$1.16/\kappa$	N/A	$1.16/\kappa$	6.28
V_{io}, V_{oi} in (5,0)@(15,0)			$V^{(r)}_{io}$, $V^{(r)}_{oi}$ in (5,0)@(15,0) at $\kappa = 2$	
$g^2_{E+D-D-E+}/\upsilon_{FC}$, $g^2_{C+E+E+C+}/\upsilon_{FC}$, $g^2_{C+E'+E'+C+}/\upsilon_{FC}$	$41.69/\kappa$	N/A	0.63, 2.43[a]	0.63,2.43

[a] The screened values of V_{io} and V_{oi} are not the same, since the former corresponds to the inner tube while the latter corresponds to the outer tube.

Since $2\pi/a$ is the Brillouin zone, the term inside the bracket is just the minimum difference in momentum, dk. So the summation over k can be replaced by an integral:

$$\Pi(q) = \frac{2}{2\pi}\int_k \frac{f(\varepsilon_{k+q}) - f(\varepsilon_k)}{\varepsilon_{k+q} - \varepsilon_k}\,\mathrm{d}k. \tag{B.3}$$

First consider the states around $+k_F$. Here we have: $\varepsilon_{k+q} = \upsilon_F(k+q-k_F)$, $\varepsilon_k = \upsilon_F(k-k_F)$, and since the Fermi–Dirac distribution function can be simplified to step function, $f(E) = 1-\theta(E)$, it follows that

$$\begin{aligned}\Pi(q) &= \frac{2}{2\pi}\int_k \frac{f(\upsilon_F(k+q-k_F)) - f(\upsilon_F(k-k_F))}{\upsilon_F(k+q-k_F) - \upsilon_F(k-k_F)}\,\mathrm{d}k \\ &= \frac{2}{2\pi}\int_k \frac{-\theta(\upsilon_F(k+q-k_F)) + \theta(\upsilon_F(k-k_F))}{\upsilon_F q}\,\mathrm{d}k.\end{aligned} \tag{B.4}$$

This integral is easy to perform. Around $+k_F$, the integral is only non-zero if $k < k_F$ and $q > 0$:

$$\Pi(q) = \frac{2}{2\pi}\int_{k=k_F-q}^{k=k_F} \frac{-\theta\left(\upsilon_F(k+q-k_F)\right)+\theta\left(\upsilon_F(k-k_F)\right)}{\upsilon_F q}\,\mathrm{d}k = -\frac{2}{2\pi}\frac{k}{\upsilon_F q}\Big|_{k_F-q}^{k_F} = \frac{-2}{2\pi}\frac{1}{\upsilon_F}. \quad \text{(B.5)}$$

For $k > k_F$ and $q < 0$, we have

$$\Pi(q) = \frac{2}{2\pi}\int_{k=k_F}^{k=k_F-q} \frac{-\theta\left(\upsilon_F(k+q-k_F)\right)+\theta\left(\upsilon_F(k-k_F)\right)}{\upsilon_F q}\,\mathrm{d}k = \frac{2}{2\pi}\frac{k}{\upsilon_F q}\Big|_{k_F}^{k_F-q} = \frac{-2}{2\pi}\frac{1}{\upsilon_F}. \quad \text{(B.6)}$$

Hence the result is $\Pi(q) = -\frac{1}{\pi\upsilon_F}$. Because the integral over k should also include the states around $-k_F$, this result should be doubled. Therefore we get the final answer: $\Pi(q) = -\frac{2}{\pi\upsilon_F}$.

Appendix C. Derivation of scaling equations

The two-loop RG is a powerful method in treating divergent diagrams in perturbation expansion of interaction vertices. Such perturbation expansion of the interaction vertices is performed up to two-loop order, which will generate $g^2\ln(\omega/E_0)$ and $g^3\ln(\omega/E_0)$ terms after integrating the internal momentum and energy variables, which can be seen to diverge as the energy ω (or temperature) decreases to zero. Here E denotes the cutoff energy. Renormalization scales the cutoff energy E_0 to a smaller value E_0'. To maintain the physical properties unchanged, all states between E_0 and E_0' should be integrated over, with the effect of these eliminated states grouped into the renormalization of the coupling constants. Such scaling equations for the coupling constants dictate their behavior as the cutoff energy ($\ln(\omega/E_0)$) decreases towards zero.

Following the standard multiplicative RG method [42–47], the scaling equations for the electron–electron coupling constants are as follows:

$$g_n^{i'}\widetilde{\Gamma}_n^i\left(\frac{k}{k_0'},\frac{\omega}{E_0'},g_n^{i'}\right)d_m^2\left(\frac{k}{k_0'},\frac{\omega}{E_0'},g_n^{i'}\right) = g_n^i\widetilde{\Gamma}_n^i\left(\frac{k}{k_0},\frac{\omega}{E_0},g_n^i\right)d_m^2\left(\frac{k}{k_0},\frac{\omega}{E_0},g_n^i\right), \quad \text{(C.1)}$$

$$\Gamma_n^{\alpha\beta\gamma\delta}(k,\omega) = g_n^1\widetilde{\Gamma}_n^1\left(\frac{k}{k_0},\frac{\omega}{E_0}\right)\delta_{\alpha\gamma}\delta_{\beta\delta} - g_n^2\widetilde{\Gamma}_n^2\left(\frac{k}{k_0},\frac{\omega}{E_0}\right)\delta_{\alpha\delta}\delta_{\beta\gamma}, \quad \text{(C.2)}$$

$$G_m(k,\omega) = d_m\left(\frac{k}{k_0},\frac{\omega}{E_0}\right)G_m^{(0)}(k,\omega). \quad \text{(C.3)}$$

Here $g_n^{i'}$ and g_n^i stand for coupling constants with scaled and original energy cutoff, respectively. The dimensionless interaction vertices $\widetilde{\Gamma}_n^i$ used in equation (C.1) are defined in equation (C.2), and the dimensionless Green's functions d_m ($m = \mathrm{A}, \mathrm{B}, \ldots \mathrm{E}, \mathrm{E}'$) are defined in equation (C.3). The G_m and $G_m^{(0)}$ are dressed and free particle Green's function, respectively. The scaling equations (C.1)–(C.3) describe the change in the coupling constants as the energy cutoff E_0 scales to a smaller value E_0'. With this method, we can perform RG analysis up to any order. This point is important, as we have pointed out that the first order RG is insufficient to obtain reliable results in the attractive region. Hence in this work the vertices and self-energy of electron Green's functions are expanded up to two loops, as shown in figures C.1 and C.2. Collecting all possible diagrams in figures C.1 and C.2, and substitute them into equations

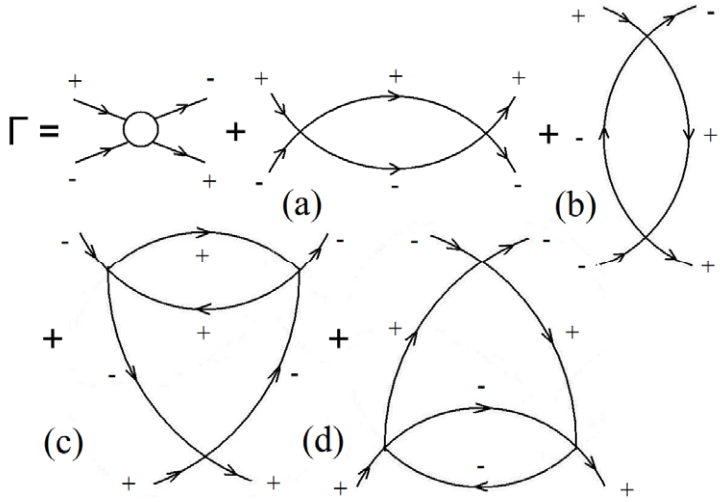

Figure C.1. Expansion of the interaction vertices. The '+' and '−' signs denote right-moving and left-moving electrons, respectively. For the first order RG, only diagrams in (a) and (b) are taken into account; while for the second order RG, we need to consider those in (c) and (d) as well. Such new diagrams eliminate the divergence in the coupling constants, and eliminate the unphysical 'phase transition' in the first order RG.

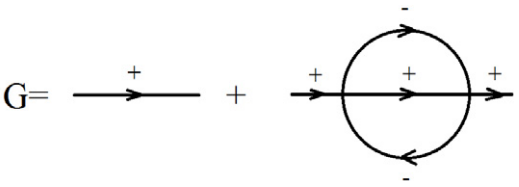

Figure C.2. The self-energy of electron Green's function taken into account in the second order RG. With such diagrams, dimensionless Green's functions d_m can be calculated.

(C.1)–(C.3), the RG scaling equations are obtained. In our derivation the differences in the Fermi velocities of the different CNTs are neglected, since in two-loop RG the difference is continuously reduced in the scaling process [23, 47].

The detailed RG equations are similar to those presented in [23], hence they will not be repeated here. The scaling equations for the inner (n,n) CNT and the outer $(n+5,n+5)$ CNT are the same, and the coupling constants of the inner tube are actually decoupled from the outer tube. The inter-tube couplings cancel each other due to our initial setting. The existence of the outer tube plays a simple role: it reduces the initial values of the forward scattering coupling constants. In both DWCNT systems, we find that the inter-tube couplings are only associated with the second order terms, i.e. the $g^3 \ln(\omega/E_0)$ terms. This is because the first order terms (the $g^2 \ln(\omega/E_0)$ ones) are only associated with inter-tube tunneling, which is considered to be negligible in our case. With second order scaling equations, we are able to calculate the response functions and the ground state properties.

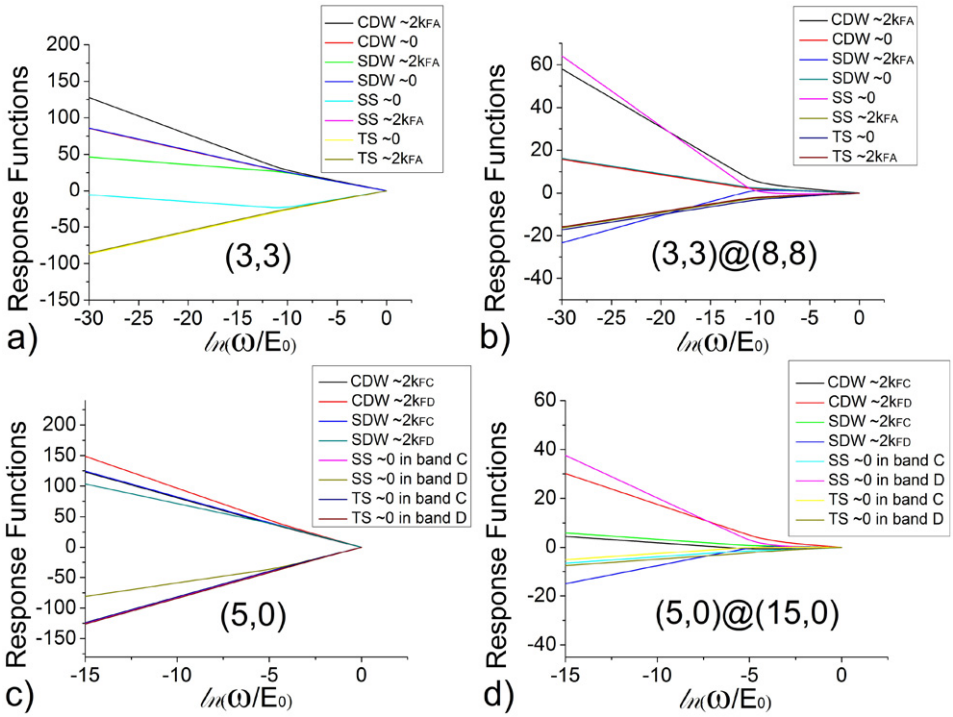

Figure D.1. The response functions of (a) single (3,3) CNT, (b) (3,3) inside (3,3)@(8,8) DWCNT, (c) single (5,0) CNT and (d) (5,0) inside (5,0)@(15,0) DWCNT, evaluated at $\kappa = 2$.

Appendix D. The response functions

Here we show all four types of response functions, namely the CDW, the SDW, the SS and the TS in single (3,3) and (5,0) CNTs, as well as those associated with the inner tube for the (3,3)@(8,8) and (5,0)@(15,0) DWCNTs (figure D.1).

For the (3,3)@(8,8) DWCNT, under the condition $\omega \to 0$, for CDW order in both the inner and outer response functions scales as $N_{\mathrm{A+B+B+A+}}(q=0) \sim (\omega/E_0)^{-0.72}$ and $N_{\mathrm{A+A-A-A+}}(q = 2k_{\mathrm{FA}}) \sim (\omega/E_0)^{-2.72}$, while for the SDW channel we have $\chi_{\mathrm{A+B+B+A+}}(q=0) \sim (\omega/E_0)^{-0.72}$ and $\chi_{\mathrm{A+A-A-A+}}(q = 2k_{\mathrm{FA}}) \sim (\omega/E_0)^{1.28}$. For the SS channel, we have $\Delta_{\mathrm{S,A+B+B+A+}}(q = 2k_{\mathrm{FA}}) \sim (\omega/E_0)^{0.72}$ and $\Delta_{\mathrm{S,A+A-A-A+}}(q=0) \sim (\omega/E_0)^{-3.28}$, and for the TS channel, $\Delta_{\mathrm{T,A+B+B+A+}}(q = 2k_{\mathrm{FA}}) \sim (\omega/E_0)^{0.72}$ and $\Delta_{\mathrm{T,A+A-A-A+}}(q=0) \sim (\omega/E_0)^{0.72}$. Hence the most divergent response function is the SS at $q = 0$ in band A.

For the individual (3,3) CNT, the results are as follows. For the $q \sim 0$ fluctuations, the response function for the CDW order is $N_{\mathrm{A+B+B+A+}}(q=0) \sim (\omega/E_0)^{-3.04}$, for SDW order is $\chi_{\mathrm{A+B+B+A+}}(q=0) \sim (\omega/E_0)^{-3.04}$, while for singlet and TS the response functions scale as $\Delta_{\mathrm{S,A+B+B+A+}}(q=0) \sim (\omega/E_0)^{3.04}$ and $\Delta_{\mathrm{T,A+B+B+A+}}(q=0) \sim (\omega/E_0)^{3.04}$, respectively. For $q \sim 2\mathrm{k}_{\mathrm{FA}}$ fluctuations, the corresponding response functions are: for CDW order, $N_{\mathrm{A+A-A-A+}}(q = 2k_{\mathrm{FA}}) \sim (\omega/E_0)^{-5.04}$, for the SDW order, $\chi_{\mathrm{A+A-A-A+}}(q = 2k_{\mathrm{FA}}) \sim (\omega/E_0)^{-1.04}$, for singlet and TS response functions, $\Delta_{\mathrm{S,A+A-A-A+}}(q = 2k_{\mathrm{FA}}) \sim (\omega/E_0)^{-0.96}$ and $\Delta_{\mathrm{T,A+A-A-A+}}(q = 2k_{\mathrm{FA}}) \sim (\omega/E_0)^{3.04}$.

For the individual (5,0) CNT, the response functions scaling are as follows: $N_{\mathrm{C+C-C-C+}}(q=2k_{\mathrm{FC}})\sim(\omega/E_0)^{-8.43}$, $N_{\mathrm{D+D-D-D+}}(q=2k_{\mathrm{FD}})\sim(\omega/E_0)^{-10.43}$, $\chi_{\mathrm{C+C-C-C+}}(q=2k_{\mathrm{FC}})\sim(\omega/E_0)^{-8.43}$ and $\chi_{\mathrm{D+D-D-D+}}(q=2k_{\mathrm{FD}})\sim(\omega/E_0)^{-6.43}$. The superconducting responses with the same nesting vectors are $\Delta_{\mathrm{S,C+C-C-C+}}(q=0)\sim(\omega/E_0)^{8.43}$, $\Delta_{\mathrm{S,D+D-D-D+}}(q=0)\sim(\omega/E_0)^{4.43}$, $\Delta_{\mathrm{T,C+C-C-C+}}(q=0)\sim(\omega/E_0)^{8.43}$ and $\Delta_{\mathrm{T,D+D-D-D+}}(q=0)\sim(\omega/E_0)^{8.43}$.

For the (5,0)@(15,0) DWCNT, we have for the CDW orders in the inner (5,0): $N_{\mathrm{C+C-C-C+}}(q=2k_{\mathrm{FC}})\sim(\omega/E_0)^{-0.52}$, $N_{\mathrm{D+D-D-D+}}(q=2k_{\mathrm{FD}})\sim(\omega/E_0)^{-2.52}$, and in the outer (15,0): $N_{\mathrm{E+E-E-E+}}(q=0)\sim(\omega/E_0)^{-0.85}$. For the SS channel, we have $\Delta_{\mathrm{S,C+C-C-C+}}(q=0)\sim(\omega/E_0)^{0.52}$, $\Delta_{\mathrm{S,D+D-D-D+}}(q=0)\sim(\omega/E_0)^{-3.48}$, and $\Delta_{\mathrm{S,E+E-E-E+}}(q=0)\sim(\omega/E_0)^{0.85}$.

References

[1] Bohnen K P, Heid R, Liu H J and Chan C T 2004 *Phys. Rev. Lett.* **93** 245501
[2] Connetable D, Rignanese G M, Charlier J C and Blase X 2005 *Phys. Rev. Lett.* **94** 015503
[3] Singer P M, Wzietek P, Alloul H, Simon F and Kuzmany H 2005 *Phys. Rev. Lett.* **95** 236403
[4] Dora B, Gulacsi M, Simon F and Kuzmany H 2007 *Phys. Rev. Lett.* **99** 166402
[5] Fernandez-Serra M V and Blase X 2008 *Phys. Rev.* B **77** 195115
[6] Bohnen K P, Heid R and Chan C T 2008 *Phys. Rev.* B **77** 235407
[7] Tang Z K, Zhang L, Wang N, Zhang X X, Wen G H, Li G D, Wang J N, Chan C T and Sheng P 2001 *Science* **292** 2462
[8] Wang Z *et al* 2010 *Phys. Rev.* B **81** 174530
[9] Kociak M, Kasumov A Y, Gueron S, Reulet B, Khodos I I, Gorbatov Y B, Volkov V T, Vaccarini L and Bouchiat H 2001 *Phys. Rev. Lett.* **86** 2416
[10] Gonzalez J 2003 *Phys. Rev.* B **67** 014528
[11] Martino A D and Egger R 2004 *Phys. Rev.* B **70** 014508
[12] Gonzalez J and Alvarez J V 2004 *Phys. Rev.* B **70** 045410
[13] Takesue I, Haruyama J, Kobayashi N, Chiashi S, Maruyama S, Sugai T and Shinohara H 2006 *Phys. Rev. Lett.* **96** 057001
[14] Murata N *et al* 2007 *Phys. Rev.* B **76** 245424
[15] Tsuneta T, Lechner L and Hakonen P J 2007 *Phys. Rev. Lett.* **98** 087002
[16] Gaididei Y B and Loktev V M 2006 *Low Temp. Phys.* **32** 1111
[17] Perfetto E and Gonzalez J 2006 *Phys. Rev.* B **74** 201403
[18] Bellucci S, Cini M, Onorato P and Perferro E 2007 *Phys. Rev.* B **75** 014523
[19] Noffsinger J and Cohen M L 2011 *Phys. Rev.* B **83** 165420
[20] Krotov Y A, Lee D H and Louie S G 1997 *Phys. Rev. Lett.* **78** 4245
[21] Sedeki A, Caron L G and Bourbonnais C 2002 *Phys. Rev.* B **65** 140515R
[22] Carperntier D and Orignac E 2006 *Phys. Rev.* B **74** 085409
[23] Zhang T, Sun M Y, Wang Z, Shi W and Sheng P 2011 *Phys. Rev.* B **84** 245449
[24] Gonzalez J and Perfetto E 2006 *Eur. Phys. J.* B **51** 571
[25] Gonzalez J and Perfetto E 2005 *Phys. Rev.* B **72** 205406
[26] Sun M Y, Hou Z L, Zhang T, Wang Z, Shi W, Lortz R and Sheng P 2012 *New J. Phys.* **14** 103018
[27] Shi W *et al* 2012 *Sci. Rep.* **2** 625
[28] Benedict L X, Crespi V H, Louie S G and Cohen M L 1995 *Phys. Rev.* B **52** 14935
[29] Egger R and Gogolin A O 1998 *Eur. Phys. J.* B **3** 281
[30] Barnett R, Demler E and Kaxiras E 2005 *Phys. Rev.* B **71** 035429
[31] Hawrylak R, Eliasson G and Quinn J J 1988 *Phys. Rev.* B **37** 10187
[32] Zheng X, Chen G H, Li Z B, Deng S Z and Xu N S 2004 *Phys. Rev. Lett.* **92** 106803
[33] Tomonaga S 1950 *Prog. Theor. Phys.* **5** 544

[34] Luttinger J M 1963 *J. Math. Phys.* **4** 1154
[35] Mattis D C and Lieb E H 1965 *J. Math. Phys.* **6** 304
[36] Delft J D and Schoeller H 1998 *Ann. Phys., Lpz.* **7** 225
[37] Gogolin A O, Nersesyan A A and Tsvelik A M 1998 *Bosonization and Strongly Correlated Systems* (Cambridge: Cambridge University Press)
[38] Voit J 1995 *Rep. Prog. Phys.* **58** 977
[39] Bockrath M, Cobden D H, Lu J, Rinzler A G, Smalley R E, Balents L and McEuen P L 1999 *Nature* **397** 598
[40] Kane C L and Fisher M P A 1992 *Phys. Rev.* B **46** 15233
[41] Charlier J C, Blase X and Roche S 2007 *Rev. Mod. Phys.* **79** 677
[42] Solyom J 1979 *Adv. Phys.* **28** 201
[43] Menyhard N and Solyom J 1973 *J. Low Temp. Phys.* **12** 529
[44] Shankar R 1994 *Rev. Mod. Phys.* **66** 129
[45] Varma C M and Zawadowski A 1985 *Phys. Rev.* B **32** 7399
[46] Penc K and Solyom J 1990 *Phys. Rev.* B **41** 704
[47] Solyom J 1973 *J. Low Temp. Phys.* **12** 547
[48] Mermin D and Wagner H 1966 *Phys. Rev. Lett.* **17** 1133
[49] Hohenberg P C 1967 *Phys. Rev.* **158** 383